

Optimization of Speed Loop Control Parameters for Doubly Fed Wind Turbines Considering Frequency Stability

Yuqi Wan

Harbin Institute of Technology (Wehai), Weihai, Shandong, China

Abstract: Frequency disturbances in the power grid frequently occur in wind power generation. To address the issue that doubly fed motors cannot effectively respond to grid frequency disturbances, leading to significant output power disturbances, this paper draws on a doubly fed wind turbine model to establish a doubly fed wind turbine frequency response model. The parameters of the speed control loop were optimized using a multi-objective optimization-weighted genetic algorithm. The study demonstrates that this model achieves frequency response while effectively reducing output power overshoot and recovery time, thereby enriching existing research findings on the transient stability of new energy grids.

Keywords: DFIG; Speed Loop; Frequency Response; PLL; Parameter Optimization

1. Introduction

To achieve the goal of carbon neutrality, renewable energy sources (RES), such as wind and solar, are increasingly replacing conventional synchronous generators (SG) in the grid. These shifts in the energy mix have dramatically altered the dynamic characteristics of the power system and have led to the development of several novel technologies. For example, in RES power generation, maximum power point tracking (MPPT) control is frequently used. The core objective of MPPT techniques in wind power generation is to maximize the wind energy capture efficiency by regulating the generator rotational speed or pitch angle, which can be adjusted by estimating the wind speed, so that the wind turbine maintains an optimal blade tip speed ratio at different wind speeds. Although these techniques can maximize the utilization of wind and solar resources, they do not respond quickly to frequency disturbances occurring on the grid side and do not have good transient stability [1]. Transient stability refers to the power system operation in a stable state encountered a large perturbation when the perturbation disappears whether it can return to the original state or reach a new acceptable stable state. As a result, the frequency regulation capability of the system decreases with the increase of renewable energy penetration, which leads to increasing concern about the stability of the power system. In this regard, it is necessary to propose new additional frequency response strategies to improve the transient stability of DFIG.

Doubly fed induction generators (DFIG) are one of the main forms of wind power generation. The rotor-side converter (RSC) in a DFIG regulates the excitation current by means of field-oriented control (FOC) to achieve independent control of active and reactive power, constant frequency and constant voltage [2,3]. This control strategy theoretically separates the electromagnetic dynamics of the generator from the grid frequency and voltage fluctuations, enabling the DFIG to operate as a

quasi-synchronous machine with adjustable power output. The DFIG is directly connected to the power system through the stator circuit and magnetic circuit inside the motor to ensure that the stator frequency is synchronized with the grid frequency. On this basis, mechanical and electrical decoupling is achieved by control devices such as RSC controllers, grid-side converter (GSC) controllers, and phase-locked loops (PLLs). [4] However, for a controller driven by state deviations, the delayed nature of the response inevitably leads to coupling between the turbine and the grid. In DFIG application scenarios, ignoring this dynamic characteristic will lead to deviations in system frequency dynamic analysis and safety assessment from the actual situation.

Existing studies have recognized this complexity and conducted research focusing on frequency response modelling and double-fed converter characterization. One study developed a generalized amplitude-phase dynamics model that accurately captures the behaviour of a doubly fed generator on various electromechanical time scales [5]. However, the model cannot be directly integrated into a full-system frequency response model and lacks the specialization of frequency dynamics analysis. It is a higher-order model that comprehensively considers the complete structure of the control machinery, but its application requires the use of system network equations to calculate in detail the amplitude and phase perturbations of the voltage at each grid point. To address these limitations, many studies have started to work on down-ordering and improving the model. However, there are different views on the focus of these improvements. Some studies have considered PLL controllers as the focus and proposed an alternative inertia control method for DFIG-based wind turbines by directly tuning the PLL response [6,7], while some studies have focused on RSC and proposed a novel stator power and frequency control method to realize the magnitude of the rotor current vector to control the stator frequency [8,9]. In addition to the above improvements in controllers, there are also studies focusing on the motor body, using a third-order model that preserves the rotor loop dynamics and mechanical equations of motion. However, due to the inverter control strategy, the time scales of both stator and rotor loop dynamics of the DFIG are milliseconds, which do not belong to the same time scale as the frequency response, which also means that the model can be further down ordered [10]. In terms of DFIG frequency response characterization, many literatures consider that the response of DFIG belongs to the category of inertia response and is analysed with the help of concepts such as inertia and damping coefficients, which are analogous to the inertia study of synchronous motors [6,11]. Although this facilitates the analysis of system frequency dynamics, the two are not equivalent. The synchronous motor inertia response originates from the spontaneous release of rotor kinetic energy, while the DFIG virtual inertia relies on the speed-frequency decoupling control, and there are essential differences between the two in terms of time constants, energy sources and nonlinear coupling characteristics [12-15]. In general, the accuracy and simplicity of the existing DFIG frequency response model has room for improvement, and the explanation of the response mechanism is not thorough enough.

Focusing on the gaps in current research, this work makes several key contributions:

1.Development of a Novel Model: A single-input single-output DFIG frequency response model is established, which reduces the model complexity while maintaining accuracy.

2.parameter optimization: The optimal parameters of the rotational speed ring are derived by a single-objective genetic algorithm.

3. Elimination of Dependency on Distributed Information: The model removes the need for distributed information such as voltage amplitudes and phase angle disturbances at the grid connection point. It uses general system information as the sole input, allowing for direct integration

into the system frequency response (SFR) model, thereby enhancing usability.

- 4. Mechanism Identification: The model reveals that the mechanism behind DFIG response to system frequency changes is the cascade effect of the PLL and speed loop.
- 5. Frequency Response Analysis: Through theoretical calculations and simulation verification, it is demonstrated that the frequency response of DFIG does not fall within the range of inertia response.
- 6. Impact Analysis: The study analyses the influence of frequency dynamics when DFIG is integrated with the electricity system

2. Frequency Response Model of DFIG

2.1 Basic Model Derivation

The research object of this paper is the response of DFIG regarding system frequency disturbances. What this novel concerns is the dynamic characteristics of DFIG in the dynamic time scale of power system frequency. This time scale is large, which belongs to the time scale extent of electromechanical transient, ranging from a few seconds to tens of seconds. To decrease the model complexity and highlight the main contradiction, make degradation and simplification for links beyond the time scale of the concerned issue according to the principle of multi-time scale system modeling and make the following assumptions [16, 17]:

- 1) Ignore the millisecond electromagnetic transient process of the internal flux linkage of the motor.
- 2) Ignore the millisecond dynamic regulation process of the inner loop of the rotor-side converter.
 - 3) Ignore the hundred millisecond DC voltage control process of the grid-side converter.
- 4) Ignore the minute-level wind speed change, considering the pitch and yaw control system does not operate during this period.
- 5) Because the frequency deviation of power system is generally small, the small disturbance linearization model is adopted.

According to the conventional modeling of the generator, the positive direction of the active power is specified to flow from the motor to the power grid. Meanwhile, the DFIG is assumed to be stator voltage vector-oriented control, and the voltage vector and the d-axis weight are combined with a delay of 90° on the q-axis. According to the typical control strategy of DFIG shown in Fig.1, the unitized model of DFIG can be established, when the controller structure is adopted, the linear expressions of the stator loop power and internal potential affected by the controller and system disturbance are as follows [18, 19]:

$$\Delta P_{s} = \frac{U_{g}E_{q}}{X_{s}E_{0}}\Delta E + \frac{E_{q}}{X_{s}}\Delta u_{g} + \frac{U_{g}E_{d}}{X_{s}}\Delta\theta_{e} - \frac{U_{g}E_{d}}{X_{s}}\Delta\theta_{g}$$
 (1)

$$\begin{bmatrix} \Delta E \\ \theta_e \end{bmatrix} = E X_{m,0} A_e B + \begin{bmatrix} 0 \\ 1 \end{bmatrix} \Delta \theta_{pll}(s) \tag{2}$$

$$B = [\Delta \omega_m(s) \quad \Delta V(s) \quad \Delta V(s) \quad \Delta \omega_g(s)]^T$$
(3)

$$E = \begin{bmatrix} \frac{E_{d,0}}{E_0} & \frac{E_{q,0}}{E_0} \\ -\frac{E_{q,0}}{E_c^2} & \frac{E_{d,0}}{E_c^2} \end{bmatrix}, \quad A_e = \begin{bmatrix} 0 & k_v & 0 & 0 \\ -\frac{L_s \omega_{pll,0} (k_{p,\omega} s + k_{l,\omega})}{L_m U_g s} & 0 & -\frac{L_s T_{em,0}^* \omega_{pll,0}}{L_m U_g} & \frac{L_s T_{em,0}^*}{L_m U_g} \Phi_{pll} \end{bmatrix}$$

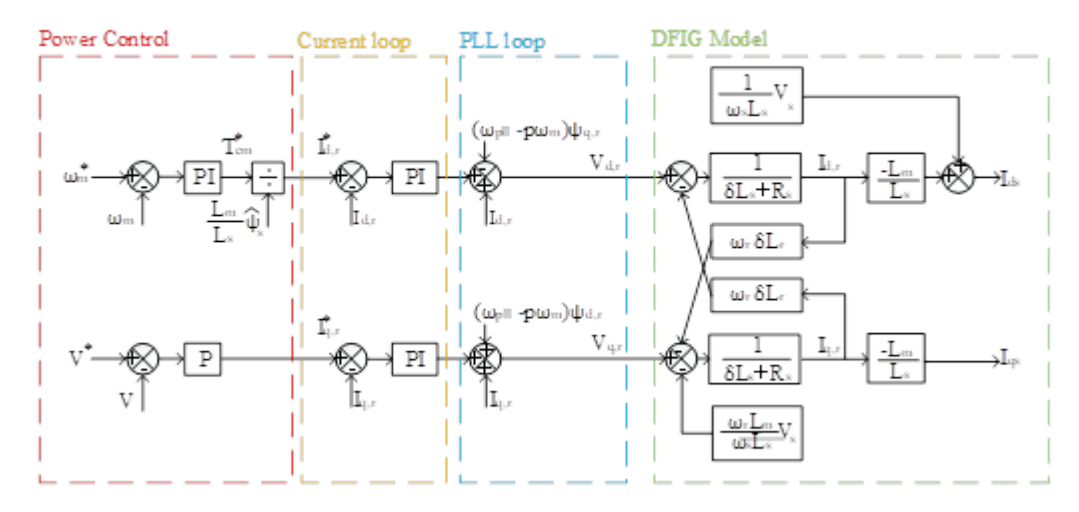


Figure 1: Basic structure of DFIG and block diagram of vector control

 Φ_{pll} is the closed-loop transfer function of PLL. The specific expression is shown in formula (4). The PLL open loop transfer function is denoted as G_{pll} .

$$\Phi_{pll} = \frac{\Delta \theta_{pll}(s)}{\Delta \theta_g(s)} = \frac{G_{pll}}{1 + G_{pll}} = \frac{k_{p,pll} u_g s + k_{i,pll} u_g}{s^2 + k_{p,pll} u_g s + k_{i,pll} u_g}$$
(4)

The relationship between the total output power P_e , stator power P_s and rotor power P_r of DFIG can be expressed as equation (5):

$$\begin{cases} P_{s} = \frac{\omega_{g}}{\omega_{m}} P_{e} \\ P_{r} = \left(1 - \frac{\omega_{g}}{\omega_{m}}\right) P_{e} \\ \frac{P_{r}}{P_{s}} = \frac{\omega_{m} - \omega_{g}}{\omega_{g}} \end{cases}$$
 (5)

On the other hand, the rotor motion equation of DFIG can be expressed as formula (6) [20]:

$$T_m - \frac{P_e}{\omega_m} - F\omega_m = 2H \frac{d\omega_m}{dt} \tag{6}$$

The process of stator power and system frequency affecting the speed change of DFIG can be obtained by linearizing the equations (5) and (6), shown in formula (7):

$$\Delta\omega_m(s) = \frac{P_s \Delta\omega_g(s) - \omega_{g,0} \Delta P_s(s)}{(2Hs + F)\omega_{g,0}^2}$$
 (7)

Substituting Eq. (7) into Eq. (2,3) to eliminate the rotational speed $\Delta\omega_m(s)$ and integrating it with Eq. (1), the complete expression of the internal potential amplitude and phase angle can be obtained as equations (8) and (9):

$$[\Delta E(s) \quad \Delta \theta_{e}(s)]^{T} = A[\Delta P_{s}(s) \quad \Delta Q(s) \quad \Delta u_{a}(s) \quad \Delta \omega_{a}(s)]^{T}$$
(8)

$$\begin{cases}
A_{11} = -\frac{E_q}{E_0} \frac{L_s}{U_g} \frac{k_{p,\omega} s + k_{i,\omega}}{(2Hs + F)s}, A_{12} = \frac{E_d X_m}{E_0} k_v, A_{13} = -\frac{E_q}{E_0} \frac{L_s T_{em}^* \omega_{pll,0}}{U_g^2} \\
A_{14} = \frac{E_q}{E_0} \left[\frac{L_s}{U_g} \frac{P_s}{\omega_{g,0}} \frac{k_{p,\omega} s + k_{i,\omega}}{(2Hs + F)s} + \frac{L_s T_{em}^* \Phi_{pll}}{U_g} \right] \\
A_{21} = -\frac{E_d}{E_0^2} \frac{L_s}{U_g} \frac{k_{p,\omega} s + k_{i,\omega}}{(2Hs + F)s}, A_{22} = -\frac{E_q X_m}{E_0^2} k_v, A_{23} = -\frac{E_d}{E_0^2} \frac{L_s T_{em}^* \omega_{pll,0}}{U_g^2} \\
A_{24} = \frac{E_d L_s}{E_0^2 U_g} \left[\frac{P_s}{\omega_{g,0}} \frac{k_{p,\omega} s + k_{i,\omega}}{(2Hs + F)s} + T_{em}^* \Phi_{pll} \right] + \frac{\Phi_{pll}}{s}
\end{cases}$$
(9)

For the convenience of description, first make the following definition, shown in equation (10):

$$G_{\omega} = \frac{k_{p,\omega}s + k_{i,\omega}}{(2Hs + F)s} \tag{10}$$

 G_{ω} is the open loop transfer function of the speed loop. Since the frequency response characterization study is concerned with the change of output power of the equipment after frequency disturbance, Eq. (1) can be linked with Eq. (8) and (9). Then, ΔE and $\Delta \theta_e$ can be eliminated to get the expression of system voltage and phase angle deviation driving the stator power of DFIG, as shown in equations. (11) and (12):

$$\Delta P_{s}(s) = A_{s} \begin{bmatrix} \Delta u_{g}(s) \\ \Delta \theta_{g}(s) \end{bmatrix}$$
(11)

$$A_s = \left[0 \quad \frac{1}{1 + G_\omega} \left[P_s \left(G_\omega s + \Phi_{pll} \right) - P_s k \left(1 - \Phi_{pll} \right) \right] \right] \tag{12}$$

It can be seen from Equation (12) that the element corresponding to the voltage disturbance in the transfer function matrix A_s is zero, and the reactive power controller has no effect on the dynamic process of frequency response. Therefore, under the principle of multi-time scale reduction, the voltage disturbance and reactive power control loop of the grid-connected point hardly affect the active power dynamic characteristics of the model on the frequency dynamic time scale. Next, by linearizing Eq. (5) and substituting it into Eq. (6), the disturbance of the total output power of DFIG can be obtained by eliminating $\Delta \omega_m$, shown as formula (13):

$$\Delta P_e(s) = \frac{P_e}{\omega_{m,0}} \left(\frac{1}{2Hs + F} - \frac{P_e}{P_s^2} \right) \left(P_s \Delta \omega_g(s) - \omega_{g,0} \Delta P_s(s) \right)$$
(13)

 $P_{e,0}$ is the steady-state value of DFIG electromagnetic power. According to Eq. (15), the total output power of DFIG is affected by both $\Delta \omega_g(s)$ and $\Delta P_s(s)$. The term $\Delta \omega_g(s)$ reflects the process that the system frequency disturbance directly affects the output power change, which is similar to the asynchronous motor and belongs to the inherent characteristics of the motor, and according to Eq. (12), $\Delta P_s(s)$ is the function of $\Delta \omega_g(s)$ (the differential of $\Delta \theta_g(s)$), which reflects the role of the controller under the disturbance of $\Delta \omega_g(s)$. Substituting Eq. (11) into Eq. (13) and Eq. (14).

$$\frac{1}{(1+G)} = 1 - \Phi \tag{14}$$

$$\Delta P_e(s) = P_e \left(\frac{P_s}{\Omega_m} \frac{1}{2Hs + F} - 1 \right) \left(1 + \frac{k}{s} \right) \frac{1}{(1 + G_\omega)(1 + G_{pll})} \Delta \omega_g(s) \tag{15}$$

The simplified expression of the reduced-order frequency response model of DFIG can be obtained after eliminating the overlapped zeros and poles in equation (15) as shown in equation (16). The model takes the global information of frequency variation $\Delta \omega_g$ as the only input, and the solution of response power does not depend on the local information such as voltage disturbance and phase disturbance at the grid-connected point. When analyzing the system frequency response, it is not necessary to construct the network equation, and the model can be directly integrated into the power SFR model to analyze the system frequency dynamics in the scenario of high proportion of wind power access, shown as equations. (16) and (17):

$$\Delta P_e(s) = -P_e \frac{\left[2Hs - \left(\frac{P_s}{\Omega_m} - F\right)\right](s+k)s^2}{C_{\omega}(s)C_p(s)} \Delta \omega_g(s) \tag{16}$$

$$\begin{cases}
C_{\omega}(s) = 2Hs + F + k_{p,\omega}s + k_{i,\omega} \\
C_{p}(s) = s^{2} + k_{p,pll}s + k_{i,pll}
\end{cases}$$
(17)

According to Eq. (16), the block diagram of DFIG total output power response system frequency deviation and the frequency response model of DFIG are shown in Fig. 2. It is worth noting that the DFIG frequency response model proposed in this paper is suitable for the wind speed range of $0 \sim 1.2$ p.u. Due to the neglect of the dynamic process of the pitch system during modeling.

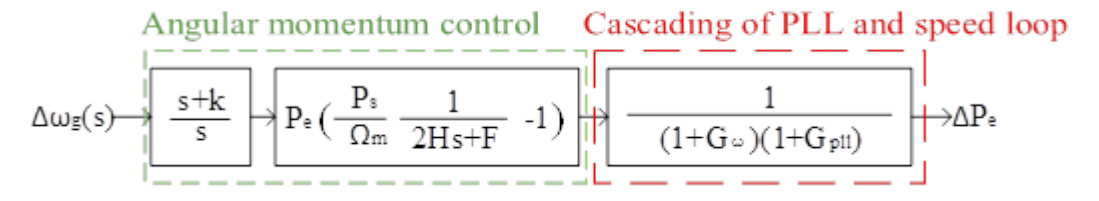


Figure 2: Frequency Response Model of DFIG.

2.2 Genetic Algorithm Optimization

In this paper, the parameters of the rotating speed ring are optimized by the weighting method of multi-objective optimization based on genetic algorithm. The multi-objective optimization problem involves multiple conflicting objective functions, and a set of solutions needs to be found to optimize all the objectives as much as possible. The weighting method converts the multi-objective into a single-objective function by assigning weights to each objective [21, 22]. The mathematical expression is shown in equation (17).

$$\begin{cases} F(x) = \sum_{i=1}^{k} w_i f_i(x) \\ \sum_{i=1}^{k} w_i = 1 \\ f_i'(x) = \frac{f_i(x) - f_{i,min}}{f_{i,max}(x) - f_{i,min}(x)} \end{cases}$$
(18)

Where w_i is the weight value; to minimize the change ΔP_e after the frequency perturbation, the above equation is used for normalization. The principle is as follows: a Cost Function is defined for evaluating the RPM loop parameters in the genetic algorithm. The cost function is based on three error metrics: the integral of squared error (ISE), the integral of absolute error (IAE) and the integral of time-weighted absolute error (ITAE). These metrics are weighed and summed up to obtain the total cost J. The objective is to minimize J. The relationship between J and ΔP_e is proportional, and when j takes the minimum value, it implies that ΔP_e is the minimum value. The first element of the input vector x is assigned to $k_{p,\omega}$ and the second element is assigned to $k_{i,\omega}$; the values of both are written to the files kp.dat and ki.dat, respectively, and three weights $w_1=0.6, w_2=0.1, w_3=0.3$, are defined for ISE, IAE, and ITAE, respectively, to run the Simulink model and to generate a variable named err (or other outputs), which contains the error signals and time information. The specific code is shown in algorithm 1.

Algorithm1

% Cost function based on ISE, IAE and ITAE w1 = 0.6; w2 = 0.1; w3 = 0.3; ISE= $w1*sum((err.signals.values).^2)$;

```
IAE=w2*sum(abs(err.signals.values));
ITAE=w3*sum(err.time .* abs(err.signals.values));
J = ISE + IAE + ITAE;
```

Through hundreds of iterations, the optimal parameters can be found: $k_{p,w} = 80.158, k_{i,w} = 2.2735$.

3. Model Simulation and Analysis

3.1 Model Advantages

This simulation uses a ramp signal starting at t=5s as input, simulating angular frequency disturbances with an amplitude of 0.02 p.u. Based on its output characteristics, the frequency response of the doubly-fed converter is designed, and the waveform changes between conventional parameters (a, b, c) and optimal parameters (d) are compared, as shown in Figure 3. Analysis of Figure 3 reveals that prior to the frequency disturbance (t=0+), the output power Δ Pe of the doubly fed inverter is zero. This indicates that at the initial moment of sudden system frequency change, the DFIG cannot provide instantaneous power support and thus does not affect the system's maximum rate of change of frequency (RoCoF) following the power disturbance. The high-pass characteristic of the DFIG's frequency response causes the output power Δ Pe to converge to zero (as shown in Equation (19)).

$$\begin{cases} \Delta P_{e}(0_{+}) = \underset{s \to \infty}{lims} P_{e,0} \frac{\left[\left(\frac{P_{s}}{\Omega_{m}} - F\right) - 2Hs\right]\left(s + \frac{E_{0}U_{g}}{X_{s}}\right)s^{2}}{s^{2}C_{\omega}(s)C_{p}(s)} = 0 \\ \Delta P_{e}(\infty) = \underset{s \to 0}{lims} P_{e,0} \frac{\left[\left(\frac{P_{s}}{\Omega_{m}} - F\right) - 2Hs\right]\left(s + \frac{E_{0}U_{g}}{X_{s}}\right)s^{2}}{s^{2}C_{\omega}(s)C_{p}(s)} = 0 \end{cases}$$

$$(19)$$

Therefore, the doubly-fed converter does not affect the final steady-state frequency deviation of the system. Regarding the impact on the maximum frequency deviation (Nadir) and frequency recovery, during the dynamic process following a disturbance (t>5s), the doubly-fed converter outputs power ΔPe with opposite polarity to the system frequency deviation Δf . This helps suppress frequency decline and promotes frequency recovery, benefiting the system.

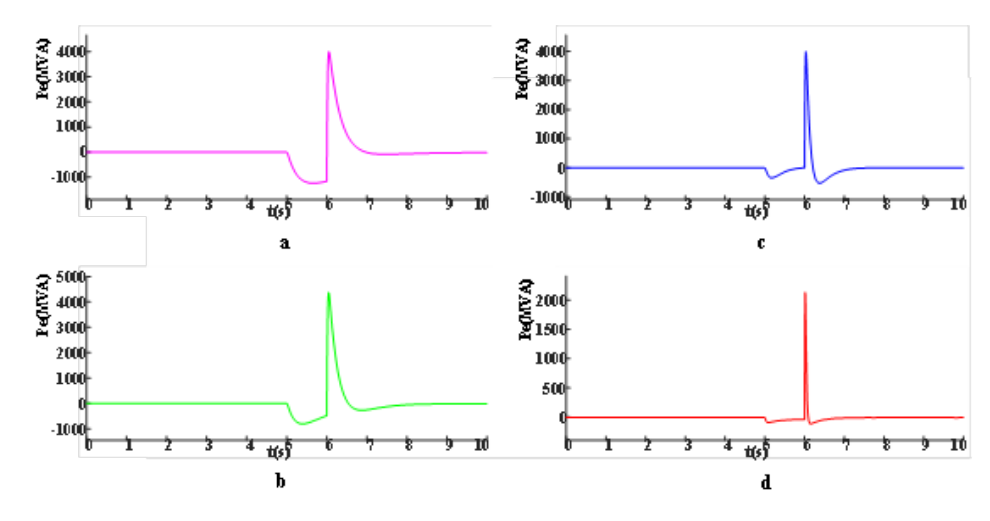


Figure 3: Model Comparison Results for Systems with Different Control Gain Design Frequencies: (a)

$$k_{p,w}=2.796, k_{i,w}=0.977;$$
 (b) $k_{p,\omega}=5.99, k_{i,\omega}=3.909;$ (c) $k_{p,\omega}=11.184, k_{i,\omega}=5.6365;$ (d) $k_{p,\omega}=80.158, k_{i,\omega}=2.2735$

3.2 Optimal Parameter Comparison

The speed-ring control coefficient critically influences dynamic frequency support capability and captured wind energy. If set excessively high, it may induce significant power fluctuations under small Δf conditions, potentially causing the DFIG to release excessive rotational energy [23]. Therefore, overly high parameters are not discussed. As shown in Figure 3, the optimal parameter model (Figure d) exhibits only half the overshoot of other parameter sets (Figures a, b, c), with minimal oscillatory fluctuations and steady-state error approaching zero. By balancing the ratio of k_p and k_i , a Pareto optimal solution is achieved in terms of speed, stability, and accuracy. This enables the doubly-fed wind turbine to rapidly provide active power support during grid frequency disturbances while avoiding abrupt power changes that exacerbate system oscillations, thereby complying with grid codes (e.g., IEEE 1547).

4. DFIG Frequency Response Model Validation

4.1 Key Links Affecting DFIG Frequency Response

The dynamic response characteristics of the DFIG to frequency perturbations depend on the coupling of the intrinsic parameters of its motor body with the behaviour of the control system. As shown in Eq. (17) and Fig. 2, the system frequency deviation significantly affects the electromagnetic power output of the DFIG by acting on the internal potential and stator self-inductance in the PLL coordinate system. By compensating the rotor current dynamics, the frequency coupling effects introduced by the PLL are eliminated, thereby improving system stability. Introducing compensation before the PI controller nearly completely eliminates the frequency coupling effects [24]. It is worth noting that the dynamic term in the model characterizing the effect of frequency deviation originates from the correlation effect introduced during the linearization of the rotational power relation $Ps/\omega g=Pe/\omega m$.

When the system frequency is perturbed, the change in the output power of DFIG will lead to a power imbalance in the rotor shaft system, which in turn triggers a dynamic change in the rotor rotational speed, a process that directly triggers the regulating effect of the speed control loop [25]. At the same time, the grid frequency deviation will drive the PLL to perform a resynchronization operation, forcing the PLL coordinate system to realign with the grid voltage phase. The coordinated action of the PLL and the speed control loop realizes the dynamic adjustment of the electromagnetic power and the rotor speed through the adjustment of the power angle [26]. During this adjustment process, the output power of the DFIG exhibits transient fluctuation characteristics, and its dynamic behaviour can be characterized by the frequency response model described in Eq. (19). It should be noted that the evolution of the potential power angle within the DFIG is determined by both the PLL and the speed loop: the PLL provides transient phase tracking for fast response to frequency deviations, while the speed loop maintains the power balance at the new slew rate through steady-state speed adjustment.

4.2 The Impact of the Speed Loop on the Model

Figure 4a, b, c, and d correspond to model simulation results with proportional coefficients of 20, 40, 60, and 80, respectively, and an integral coefficient of 2.2735. The figures reveal that power disturbances and oscillation amplitudes decrease as parameters approach optimal values, exhibiting a

diminishing trend. Increasing the proportional coefficient while keeping the integral coefficient constant typically enhances the dynamic response speed of DFIG speed-loop control systems, enabling faster suppression of external disturbances (e.g., wind speed variations, grid fluctuations). This observation successfully validates the model's accuracy, aligning with practical conditions.

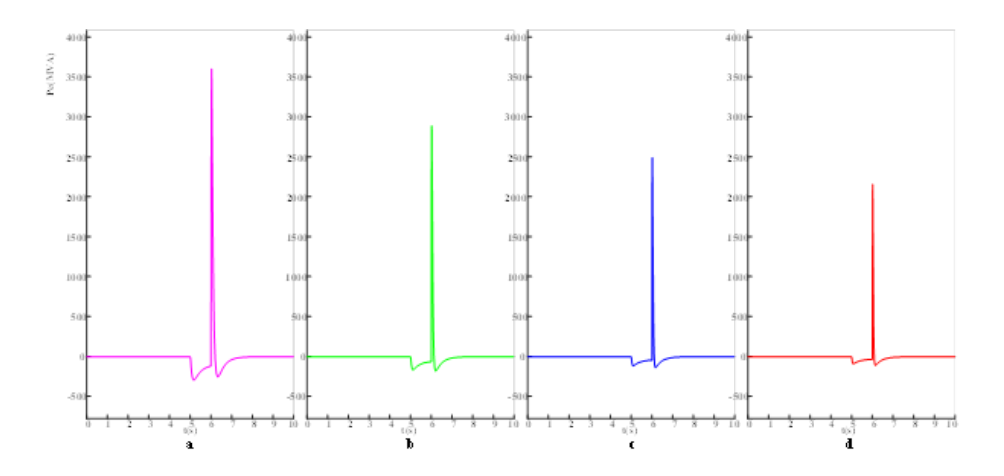


Figure 4: Different Gain Models.

Figures 5a, b, c, and d correspond to model simulation results with integral coefficients of 20, 40, 60, and 80, respectively, and a proportional coefficient of 80.158. The figures reveal that power disturbances decrease as the parameters approach the optimal values, exhibiting a diminishing trend. In the speed loop, the proportional coefficient determines the system's initial response speed, while the integral coefficient primarily serves for later correction. If unchanged, the system's initial disturbance rejection capability is mainly determined by the proportional coefficient; increasing the integral coefficient does not significantly improve dynamic performance. The lagging nature of integral control: The integral term requires time to accumulate error. Therefore, during the initial phase of disturbance occurrence (e.g., sudden wind speed changes), the integral effect has not yet fully manifested, and the disturbance's impact is still primarily determined by the proportional coefficient. This behaviour also aligns with real-world conditions.

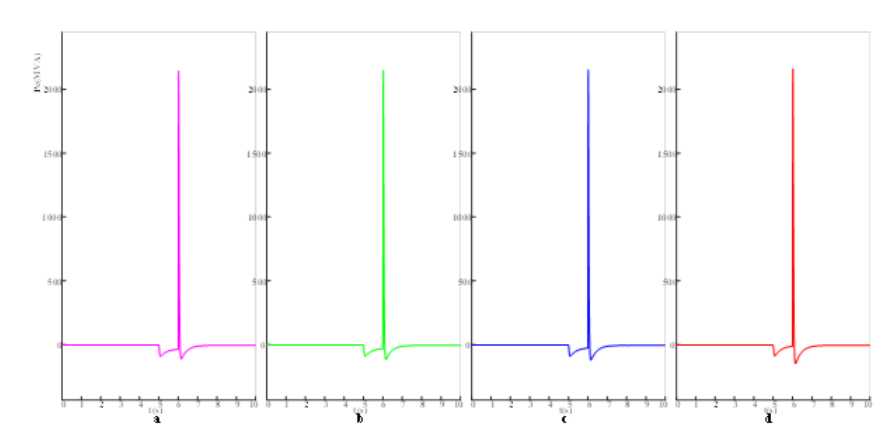


Figure 5: Different Integral Gain Models.

4.3 The Impact of the PLL Loop on the Model

The bandwidth of the PLL directly determines its proportional and integral coefficients. When

the PLL bandwidth is 0.5 Hz, the proportional and integral coefficients of the phase-locked PI controller are 4.443 and 9.87, respectively; when the bandwidth is 1 Hz, they are 8.886 and 39.478, respectively; At a bandwidth of 1.5 Hz, the proportional and integral coefficients of the phase-locked PI controller are 13.329 and 88.826, respectively; at a bandwidth of 2 Hz, they are 17.772 and 157.913. Figures 6a, b, c, and d represent the PLL bandwidth models at 0.5, 1, 1.5, and 2 Hz, respectively. As shown in Figure 6, as the PLL bandwidth increases, the model's oscillation and recovery time decrease, and its disturbance resistance strengthens.

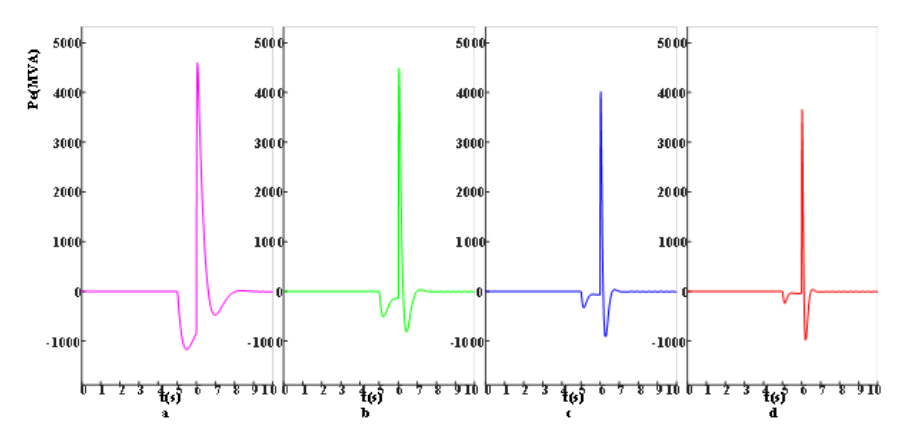


Figure 6: Different PLL Bandwidth Models.

5. Influence of DFIG Frequency Response on System Frequency Dynamics

The DFIG achieves the output power control by controlling the rotational speed and the synchronization of the d and q coordinate systems. When the controller parameters are taken at reasonable values, it will be beneficial to reduce the maximum frequency deviation, and the effect of this frequency response model is analyzed in the following for different system inertia. The frequency response model is shown in Figure 7. In the figure: ΔP is the active power disturbance in the power system; H_s is the system inertia; k_D and $k_G/(\tau s+1)$ characterize the frequency characteristics of the load and generator, respectively, while the branch in the dashed box characterizes the frequency response characteristics of the DFIG, where k_D is the frequency regulation effect coefficient of the load, k_G is the regulation coefficient, and τ is the delay coefficient of the corresponding frequency fluctuation of the governor.

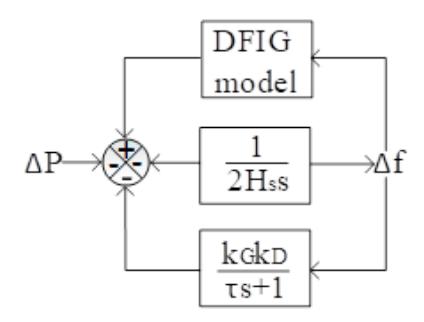


Figure 7: The Frequency Response Model.

Figure 8(a) and (b) compare the frequency response curves of the system before and after whether the DFIG characteristics are considered at different values of H. From the figure, when the inertia of the system is large, the frequency response characteristics of DFIG have little effect on the system frequency dynamics; however, when the inertia of the system is small, the effect of DFIG on

the frequency dynamic characteristics of the system is not negligible. For example, when Hs = 9, whether or not to consider the DFIG characteristics of the analyzed system frequency characteristics of the influence is not significant; and when Hs = 3, after considering the DFIG characteristics of the system, the actual maximum frequency difference is 5.555 * 10e + 06VA, compared with the non-consideration of the system's 6.904 * 10e + 06VA, a decrease of 19.54%. For the system with low inertia, ignoring the DFIG characteristics will make the analysis of the frequency dynamic characteristics of the power system have a large deviation, which will lead to the assessment of the power system inertia demand deviation from the actual situation.

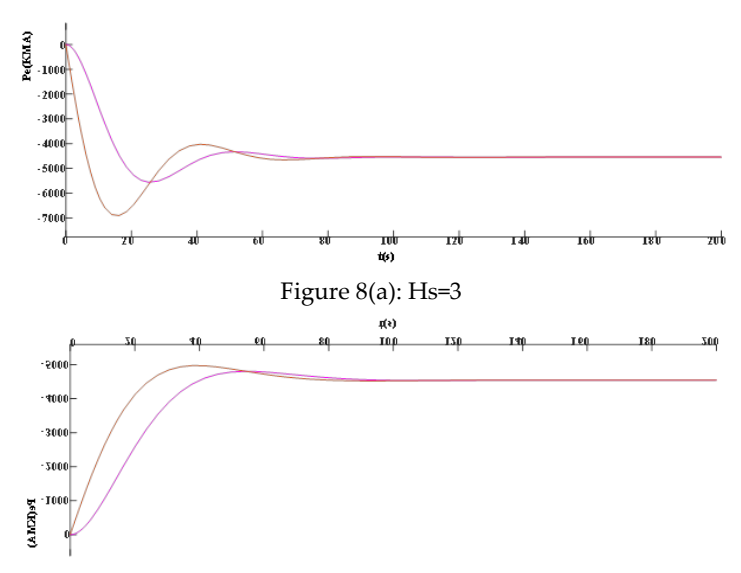


Figure 8(b): Hs=9

6. Conclusion

This paper presents a dynamic model of DFIG that responds to system frequency disturbances using only global frequency disturbance information as input. A genetic algorithm was employed to optimize the speed loop parameters, and the results were compared with those obtained using conventional parameters. Based on this optimized model, an in-depth study of the DFIG's frequency response was conducted, revealing that its response mechanism stems from the cascaded coupling effects between PLL and the outer-loop controller (particularly the speed loop). Its response characteristics exhibit fundamental differences from the inertial response of traditional synchronous machines. The main conclusions are as follows:

- (1) The frequency response of DFIG is mainly affected by the cascading effect of PLL and speed control loop. The frequency response of DFIG is mainly dominated by the cascading effect of PLL and speed control loop. Reducing the bandwidth of PLL or speed control loop will weaken DFIG's ability to resist frequency disturbance.
- (2) Changes in system frequency will cause fluctuations in its slope and power output. Through closed-loop control, the PLL and speed loop resynchronize after disturbances to adapt to the new system frequency and mitigate the negative impact of frequency disturbances on output power.
- (3) The frequency response of the DFIG exhibits a high-pass characteristic: it generates a response only in the transient phase of the system frequency change (i.e., when there exists a rate of change); when the system frequency reaches the steady state (even if there exists a steady state frequency difference), its response output decays to zero. Critically, the change in output power, ΔPe , is not

proportional to the system RoCoF. Therefore, this response characteristic does not belong to the conventional inertial response and does not contribute to the improvement of the maximum RoCoF at the onset of the perturbation (t=0+).

- (4) During the dynamic change of system frequency, the DFIG can provide a short-time active power output with opposite polarity to the frequency deviation Δf . This characteristic is beneficial for system frequency recovery, especially in low-inertia systems, and should not be ignored. The frequency response of the DFIG helps to improve the maximum frequency nadir of the system when the controller parameters are properly configured.
- (5) The optimized parameter model can effectively reduce oscillations and recovery time, greatly reducing the impact of frequency disturbances on output power.

References

- [1] Y. Zou, M. E. Elbuluk and Y. Sozer, "Stability Analysis of Maximum Power Point Tracking (MPPT) Method in Wind Power Systems," in IEEE Transactions on Industry Applications, vol. 49, no. 3, pp. 1129-1136, May-June 2013, doi: 10.1109/TIA.2013.2251854.
- [2] L.M. Fernandez, C.A. Garcia, F. Jurado, Comparative study on the performance of control systems for doubly fed induction generator (DFIG) wind turbines operating with power regulation, Energy, Volume 33, Issue 9, 2008, Pages 1438-1452, ISSN 0360-5442, https://doi.org/10.1016/j.energy.2008.05.006.
- [3] H. Jeon, Y. C. Kang, J. -W. Park and Y. Il Lee, "PI Control Loop–Based Frequency Smoothing of a Doubly-Fed Induction Generator," in IEEE Transactions on Sustainable Energy, vol. 12, no. 3, pp. 1811-1819, July 2021, doi: 10.1109/TSTE.2021.3066682.
- [4] Y. Luo, J. Yao, D. Yang, H. Xie, L. Zhao and R. Jin, "Improved LVRT Strategy for DFIG-based Wind Turbine Considering RSC-GSC Interaction during Symmetrical Grid Faults," in IEEE Transactions on Energy Conversion, doi: 10.1109/TEC.2025.3538318.
- [5] M. Zhao, X. Yuan and J. Hu, "Modeling of DFIG Wind Turbine Based on Internal Voltage Motion Equation in Power Systems Phase-Amplitude Dynamics Analysis," in IEEE Transactions on Power Systems, vol. 33, no. 2, pp. 1484-1495, March 2018, doi: 10.1109/TPWRS.2017.2728598.
- [6] J. Lee, G. Jang, E. Muljadi, F. Blaabjerg, Z. Chen and Y. Cheol Kang, "Stable Short-Term Frequency Support Using Adaptive Gains for a DFIG-Based Wind Power Plant," in IEEE Transactions on Energy Conversion, vol. 31, no. 3, pp. 1068-1079, Sept. 2016, doi: 10.1109/TEC.2016.2532366.
- [7] D. Zhu, X. Guo, B. Tang, J. Hu, X. Zou and Y. Kang, "Feedforward Frequency Deviation Control in PLL for Fast Inertial Response of DFIG-Based Wind Turbines," in IEEE Transactions on Power Electronics, vol. 39, no. 1, pp. 664-676, Jan. 2024, doi: 10.1109/TPEL.2023.3319134.
- [8] C. Wu, P. Cheng, H. Nian and F. Blaabjerg, "Rotor Current Oriented Control Method of DFIG-DC System Without Stator Side Sensors," in IEEE Transactions on Industrial Electronics, vol. 67, no. 11, pp. 9958-9962, Nov. 2020, doi: 10.1109/TIE.2019.2956415.
- [9] R M, Thampatty KCS. Design and implementation of modified RSC controller for the extenuation of sub-synchronous resonance oscillations in series compensated DFIG-based WECS. Int Trans Electr Energ Syst. 2020; 30: e12396. https://doi.org/10.1002/2050-7038.12396
- [10] W. He, X. Yuan and J. Hu, "Inertia Provision and Estimation of PLL-Based DFIG Wind Turbines," in IEEE Transactions on Power Systems, vol. 32, no. 1, pp. 510-521, Jan. 2017, doi: 10.1109/TPWRS.2016.2556721.
- [11] X. Xi, H. Geng, G. Yang, S. Li and F. Gao, "Two-Level Damping Control for DFIG-Based Wind Farm Providing Synthetic Inertial Service," in IEEE Transactions on Industry Applications, vol. 54, no. 2, pp. 1712-1723, March-April 2018, doi: 10.1109/TIA.2017.2765298.

- [12] J. Liu, C. Wang, J. Zhao, B. Tan and T. Bi, "Simplified Transient Model of DFIG Wind Turbine for COI Frequency Dynamics and Frequency Spatial Variation Analysis," in IEEE Transactions on Power Systems, vol. 39, no. 2, pp. 3752-3768, March 2024, doi: 10.1109/TPWRS.2023.3301928.
- [13] Chao Jiang, Guowei Cai, Dongfeng Yang, Xiaojun Liu, Shuyu Hao, Bohan Li, Multi-objective configuration and evaluation of dynamic virtual inertia from DFIG based wind farm for frequency regulation, International Journal of Electrical Power & Energy Systems, Volume 158,2024,109956, ISSN 0142-0615, https://doi.org/10.1016/j.ijepes.2024.109956.
- [14] M. Li, W. Huang, N. Tai, L. Yang, D. Duan and Z. Ma, "A Dual-Adaptivity Inertia Control Strategy for Virtual Synchronous Generator," in IEEE Transactions on Power Systems, vol. 35, no. 1, pp. 594-604, Jan. 2020, doi: 10.1109/TPWRS.2019.2935325.
- [15] C. Sun, S. Q. Ali, G. Joos and F. Bouffard, "Design of Hybrid-Storage-Based Virtual Synchronous Machine With Energy Recovery Control Considering Energy Consumed in Inertial and Damping Support," in IEEE Transactions on Power Electronics, vol. 37, no. 3, pp. 2648-2666, March 2022, doi: 10.1109/TPEL.2021.3111482.
- [16] HE W, YUAN X M, HU J B. Inertia provision and estimation of PLL-based DFIG wind turbines. IEEE Transactions on Power Systems, 2017, 32 (1): 510-521.
- [17] KAYIKCI M, MILANOVIC J V. Dynamic contribution of DFIG-based wind plants to system frequency disturbances. IEEE Transactions on Power Systems. 2009, 24 (2): 859-867.
- [18] HUANG, H., JU, P., PAN, X. et al. Phase–amplitude model for doubly fed induction generators. J. Mod. Power Syst. Clean Energy 7, 369–379 (2019). https://doi.org/10.1007/s40565-018-0450-0.
- [19] X. Gao, Z. Xie, M. Li, S. Yang and X. Zhang, "Analysis and Mitigation of Electromechanical Oscillations in Drivetrain for Hybrid Synchronization Control of DFIG-Based Wind Turbines," in IEEE Transactions on Power Electronics, vol. 39, no. 3, pp. 3002-3013, March 2024, doi: 10.1109/TPEL.2023.3335481.
- [20] Marler, R., Arora, J. Survey of multi-objective optimization methods for engineering. Struct Multidisc Optim 26, 369–395 (2004). https://doi.org/10.1007/s00158-003-0368-6.
- [21] S. Huang, D. Yang, C. Zhong, S. Yan and L. Zhang, "An Improved Ant Colony Optimization Algorithm for Multi-Agent Path Planning," 2021 International Conference on Networking Systems of AI (INSAI), Shanghai, China, 2021, pp. 95-100, doi: 10.1109/INSAI54028.2021.00028.
- [22] Marler, R., Arora, J. Survey of multi-objective optimization methods for engineering. Struct Multidisc Optim 26, 369–395 (2004). https://doi.org/10.1007/s00158-003-0368-6.
- [23] S. Huang, D. Yang, C. Zhong, S. Yan and L. Zhang, "An Improved Ant Colony Optimization Algorithm for Multi-Agent Path Planning," 2021 International Conference on Networking Systems of AI (INSAI), Shanghai, China, 2021, pp. 95-100, doi: 10.1109/INSAI54028.2021.00028.
- [24] X. Xiong, B. Luo, L. Li, Z. Sun and F. Blaabjerg, "Impedance Reshaping Method of DFIG System Based on Compensating Rotor Current Dynamic to Eliminate PLL Influence," in IEEE Transactions on Power Electronics, vol. 39, no. 4, pp. 4006-4016, April 2024, doi: 10.1109/TPEL.2023.3346042.
- [25] A. Mullane and M. O'Malley, "The inertial response of induction-machine-based wind turbines," in IEEE Transactions on Power Systems, vol. 20, no. 3, pp. 1496-1503, Aug. 2005, doi: 10.1109/TPWRS.2005.852081.
- [26] Y. Zhou, D. Zhu, J. Hu, X. Zou and Y. Kang, "Phase Step Control in PLL of DFIG-Based Wind Turbines for Ultrafast Frequency Support," in IEEE Transactions on Power Electronics, vol. 40, no. 1, pp. 51-56, Jan. 2025, doi: 10.1109/TPEL.2024.3448454.